RESEARCH ARTICLE

In situ Observation of Ternary Eutectic Growth in a Directionally Solidified Mo–Si–B Alloy Using High-Energy Synchrotron X-Rays

Georg Hasemann,* Linye Zhu, Katja Hauschildt, Malte Blankenburg, Shuntaro Ida, Florian Pyczak, Kyosuke Yoshimi, and Manja Krüger

Herein, synchrotron-generated high-energy X-ray is used to study growth behavior at the liquid–solid transition of multicomponent alloys during in situ directional solidification experiments at Deutsche Elektronen-Synchrotron (DESY), Hamburg, Germany. The unique "FlexiDS" sample environment is used to directly investigate crystal growth of a ternary eutectic Mo–17.5Si–8B alloy. During the directional solidification process, high-energy X-rays with a photon energy of 100 keV ($\lambda = 0.124$ Å) are used in transmission to obtain Debye–Scherrer diffraction rings. The diffraction rings were obtained within the liquid phase, the liquid–solid interphase and the solidified eutectic crystals by scanning through the respective observation volume of interest. The results provide strong evidences for a coupled ternary eutectic growth of the phases Mo_{SS}, Mo_3Si, and Mo_5SiB_2, which can be directly observed during in situ experiments for the first time.

1. Introduction

Molybdenum-based alloys such as molybdenum silicides and Mo–Si–B alloys are seen as very promising candidates for the next-generation turbine blade material beyond the capability of state-of-the-art Ni-based superalloys and are therefore studied extensively over the past two decades. Mo–Si–B alloys in particular, combine excellent creep properties and acceptable oxidation resistance at high and ultrahigh temperatures.[1–3]

The microstructure formation and the materials' properties strongly depend on the processing route of Mo–Si–B alloys. According to Schneibel et al.,[4] the microstructure–property relationship can be divided in two major cases: i) The alloy's microstructure is composed of a Mo_{SS} matrix with embedded intermetallic particles and a relatively coarse microstructure. Such an alloy would exhibit high fracture toughness values due to the ductile Mo_{SS} matrix phase which would be strengthened by a classical coherent or partially coherent second phase hardening mechanism. The major disadvantages of such an alloy would be a quite poor oxidation and creep resistance, due to the high Mo_{SS} volume fraction. ii) The alloy's microstructure is composed of an intermetallic matrix in which the ductile Mo_{SS} phase would be embedded. In case of a coarse-grained microstructure with relatively large particles of the ductile Mo_{SS} phase, the creep behavior can be influenced in a positive way. In contrast, if the intermetallic matrix contains only small particles of the Mo_{SS} phase then the oxidation resistance of the alloy can be increased. Thus, a holistic approach considering the alloy composition (affecting the phase distribution and volume fraction of phases) and the alloys microstructure has to be pursued to achieve the desired mechanical and oxidation properties to tailor alloys for specific applications.[4] Hence, different manufacturing strategies have been developed over the years to produce various types of Mo–Si–B alloys including powder metallurgy (PM), with powders produced either via gas atomization (GA)[5–7] or mechanical alloying (MA),[8–10] ingot metallurgy (IM),[11,12] directional solidification (DS),[13–17] and very recently additive manufacturing (AM).[18]

DS offers the possibility to directly control the growth morphology of the microstructure basically by two parameters: the

Dr. G. Hasemann, Prof. M. Krüger
Institute of Materials and Joining Technology
Otto-von-Guericke University Magdeburg
Universitätsplatz 2, Magdeburg 30106, Germany
E-mail: georg1.hasemann@ovgu.de

L. Zhu, Dr. S. Ida, Prof. K. Yoshimi
Department of Materials Science
Graduate School of Engineering
Tohoku University
6-6-02 Aramaki Aza Aoba, Sendai, Miyagi 980-8579, Japan

Dr. K. Hauschildt, Dr. M. Blankenburg, Prof. F. Pyczak
Institute of Materials Physics
Helmholtz-Zentrum Geesthacht
Max-Planck-Str. 1, Geesthacht 21502, Germany

Dr. M. Blankenburg
Deutsche Elektronen-Synchrotron (DESY)
FS-PETRA-D
Notkestr. 85, Hamburg 22603, Germany

The ORCID identification number(s) for the author(s) of this article can be found under https://doi.org/10.1002/adem.202100111.

**ADVANCED
SCIENCE NEWS**

www.advancedsciencenews.com

**ADVANCED
ENGINEERING
MATERIALS**

www.aem-journal.com

temperature gradient over the solidification front, G, and the growth rate, v.[19] In general, G is determined by the DS system. It depends on technical parameters such as the design and cooling of sample chucks and/or thermal conductivity of the sample material and is therefore difficult to control actively. However, v can be easily manipulated and adjusted during the DS process. For ternary eutectic Mo–Si–B alloys, a microstructure refinement by increasing the growth rate has been reported earlier.[16,17]

Mason et al.[13] investigated a directionally solidified eutectic composition consisting of the two phases $MoSi_2$ and Mo_5Si_3, varying the solidification velocities from 25 to 210 mm h^{-1}. They achieved a lamellar crystal morphology parallel to the growth direction and concluded that the cooperative growth of $MoSi_2$ and Mo_5Si_3 structures proceeded in a similar manner as the eutectoid growth of pearlite in austenite. An improvement of creep strength at 1300 °C and higher temperatures was found with decreased lamellar spacing of the $MoSi_2$–Mo_5Si_3 eutectic.[20]

Ito et al.[14] investigated different multiphase DS alloys with either a two-phase Mo_{SS}–Mo_5SiB_2 or a three-phase (Mo, Nb)$_{SS}$–Mo_5Si_3–Mo_5SiB_2 eutectic microstructure. Using an optical float zone method, they achieved a Mo_{SS}–Mo_5SiB_2 two-phase microstructure in the alloy Mo–9Si–18B (if not stated otherwise, all compositions are given in at%) using a solidification rate of less than 5 mm h^{-1}. It was observed that the Mo_{SS} phase appears in two characteristic microstructures, either of a short rod-like morphology or as coarse particles. The three-phase (Mo,Nb)$_{SS}$–Mo_5Si_3–Mo_5SiB_2 microstructure of the alloy (Mo,Nb)–19.5Si–3B could be refined by increasing the growth rate up to 200 mm h^{-1} which results in a typical lamellar eutectic structure. However, no significant dependence of room temperature fracture toughness and strength at 1500 °C on the DS microstructure has been observed at solidification rate between 2.5 and 200 mm h^{-1} by Ito et al.[14]

Wang et al.[21] reported on the microstructure and oxidation behavior of the directionally solidified Mo–10Si–14B alloy. Coarse (cell sizes >100 μm) three-phase Mo_{SS}–Mo_3Si–Mo_5SiB_2 microstructures were obtained at growth rates of 10 and 30 mm h^{-1}. Due to the DS process, this coarse microstructure results in a poor oxidation resistance caused by catastrophic oxidation of large Mo_{SS} regions (the so-called pesting phenomenon). In contrast, a refinement of the microstructure by increasing the growth rate corroborates the findings of Ito et al.[14] and leads to an increased oxidation resistance. However, a distinct microstructural alignment with respect to the growth direction obtained by the processing route of Wang et al.[21] is difficult to distinguish, in contrast to the new DSed eutectic alloy which is investigated in this work.

In terms of (ternary) eutectic alloys one has to note here, that they are especially suited and preferred for the DS process as they represent the lowest melting point of an alloy system. Due to the direct liquid–solid phase transition, eutectics provide excellent controllability of the microstructure formation, i.e., varying the lamellar spacing or fiber diameter of eutectic systems by adjusting the DS parameters such as growth velocity and rotation speed.[22]

This study focuses exclusively on the ternary eutectic growth, microstructure and texture formation during DS of the eutectic alloy Mo–17.5Si–8B. During the in situ diffraction experiments at the German synchrotron source at Deutsche Elektronen-

Synchrotron (DESY), Hamburg, special interest was paid to the liquid–solid transformation and the eutectic decomposition of the liquid phase into the three (eutectic) phases Mo_{SS}, Mo_3Si, and Mo_5SiB_2. The microstructure perpendicular and parallel to the solidification direction was analyzed and the DS textures obtained by in situ synchrotron high-energy X-ray diffraction (HEXRD) and scanning electron microscope (SEM)–electron-backscatter diffraction (EBSD) were compared.

2. Experimental Section

To produce eutectic Mo–Si–B alloys for DS, the following processing steps were applied, as shown in **Figure 1**. First, elemental starting materials were used to produce a master alloy of around 30 g per button by conventional arc-melting in an Ar atmosphere. High purity chips or granules of Mo (99.95 wt%), Si (99.999 wt%), and B (99.5 wt%) were used. To ensure good homogeneity, each button was flipped and remelted five times. In a second step, 80–90 g of the master alloy was filled in an inductively heated cold-crucible furnace (Forschungszentrum Jülich GmbH, Germany[23]) and melted in Ar atmosphere twice. For the second melting, the whole button was flipped and melted again before it was drop casted in a cylindrical copper mold with 8 mm in diameter and 90 mm in length. Prior to DS, two 90 mm-long eutectic Mo–17.5Si–8B casted rods were mounted in the DS device and joined by welding using the induction coil of the zone melting device. Thus, a sample length for the DS device of at least 150 mm could be achieved and the sample was prepared for the zone melting experiments.

DS was carried out using the FlexiDS zone melting device,[24] a worldwide unique sample environment that was specially designed to be used for DS in situ experiments at the P07 High Energy Materials Science (HEMS) beamline operated by Helmholtz-Zentrum Geesthacht at PETRA III (DESY; Hamburg, Germany). In this work, DS was carried out in an Ar atmosphere using a growth velocity of 60 mm h^{-1} and a synchronized rotation speed of 20 rpm for the feed and seed axis. The growth velocity is based on previous results of DSed Mo–17.5Si–8B.[16,17]

For the in situ HEXRD experiments, a monochromatic beam with a photon energy of 100 keV ($\lambda = 0.124$ Å) and a narrow cross section of 1×0.5 mm^2 (width and height) was used in transmission mode. A Perkin Elmer XRD 1621 flat panel detector was used to record the Debye–Scherrer diffraction patterns. The DS device can be moved in vertical direction through the beam, which enables data collection at different positions relative to the molten zone while processing. The software Fit2D[25,26] was used for azimuthal integration of the recorded 2D-diffraction patterns. For the Rietveld refinement, the upper right quarter of the detector images was used. Thus, the diffraction patterns were integrated from 0° to 90°. This quarter was least shaded by the DS machine. In addition, the mean intensities of the rings in this area are not influenced by the formed texture. This is the case, because this quarter contains the complete information of all orientations of all phases because the texture formed during solidification is a fiber texture perpendicular to the solidification front (i.e., fiber axis parallel to the vertical detector axis and the mirror plane of the fiber perpendicular to the fiber axis). Furthermore, the integrated data were normalized to the
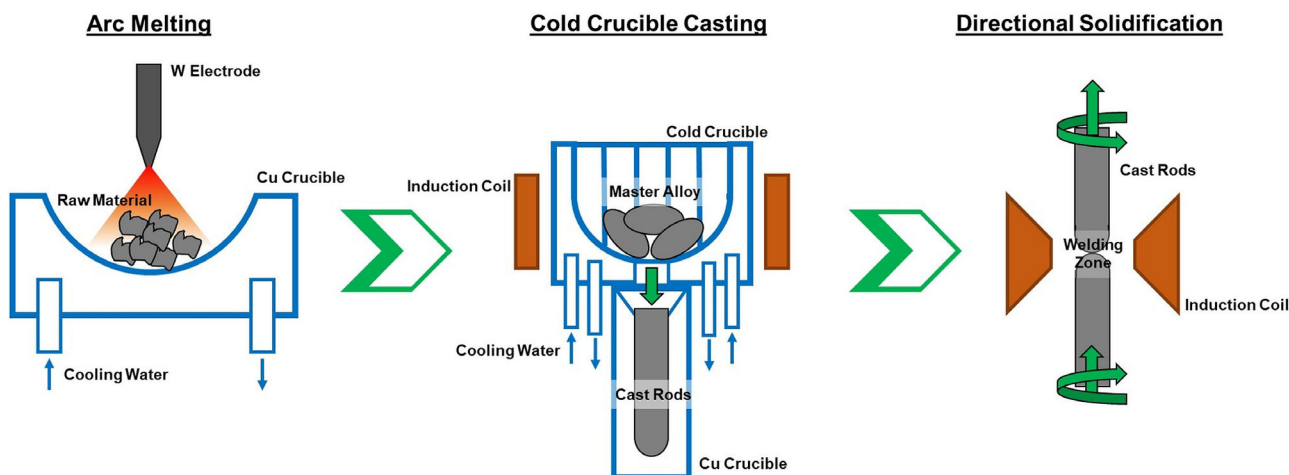
Figure 1. Scheme of the sample preparation steps applied in this work starting from master alloy preparation via arc melting, rod casting using a cold crucible furnace and DS of the casted rods.

background intensity. The resulting data files were analyzed by Rietveld refinement using the software MAUD.[27] For this, the stoichiometric compositions of the phases were used as phase prototypes. The background was fitted with a linear slope. In addition, the diffuse background caused by the melt was fitted with two Gaussian peaks at the 2Θ-positions around $3.1°$ and $5.2°$. The melt fraction was calculated based on the area under the first Gaussian peak assuming that a linear dependence exists between liquid fraction and peak area.[28,29] In addition, a texture analysis was carried out for the DSed material using the software MAUD. It was assumed that the resulting preferred orientation is a fiber texture. (The phase fractions obtained in this way agree very well with the values determined without considering texture).

To investigate the DSed microstructures, samples were cut longitudinal and transversal with respect to the growth direction via electrical discharge machining (EDM). After subsequent grinding, the specimens were finished by polishing with 3 and 1 µm alumina suspension. The polished SEM specimens were subjected to further vibratory polishing with a suspension of 40 nm polycrystalline diamond in ethylene glycol in a Buehler VibroMet 2 vibratory polisher to produce stress-free surfaces for the EBSD measurements. The microstructural observations were carried out using a SEM Zeiss Merlin (equipped with an energy-dispersive X-ray spectroscope [EDS] from Oxford Instruments) or a JEOL JSM-7800F. The SEM images were typically obtained in the backscattered electron (BSE). Crystallographic analysis, including the identification of the preferred growth directions and the potential orientation relationships between the constituent phases, was carried out by EBSD (TSL OIM Analysis software, EDAX Inc.) and orientation-imaging microscopy. Millimeter-sized areas in the middle of the samples were scanned to acquire pole figures and inverse pole figures (IPFs).

The microstructure was further investigated by transmission electron microscopy (TEM) using a JEOL JEM-2100 instrument operated at 200 kV. Specimens for TEM observation were carefully prethinned to a thickness of about 50 µm using SiC papers of up to 1200 grit size with water in an Ollie OP-801A

metallographic grinding-and polishing machine. Final thinning and perforation were accomplished by twin-jet electropolishing using a Struers TenuPol-5 electropolisher. Optimal thinning conditions were achieved using an electrolyte consisting of 12.5 vol% sulfuric acid and 87.5 vol% methanol at -20 to $-25\,°C$ and 30–40 V.

3. Results and Discussion

3.1. Microstructural Morphology of Directionally Solidified Mo–17.5Si–8B

Figure 2 shows the microstructure of the DSed alloy parallel (longitudinal, Figure 2a) and perpendicular (transversal, Figure 2b) to the growth direction. A well-aligned eutectic microstructure was observed that consists of a uniform eutectic cell configuration. Within the ternary eutectic cells, the Mo_3Si phase forms as the major phase and the Mo_{SS} and Mo_5SiB_2 phases retain a rod-like shape and are only slightly distorted at the cell boundaries. Detailed TEM images of the longitudinal section (Figure 2c) and the transversal section (Figure 2d) show that both phases, Mo_{SS} and Mo_5SiB_2, grew in uniform rod shapes oriented parallel to the growth direction. The Mo–17.5Si–8B master alloy was slightly hypereutectic showing very few primary Mo_5SiB_2 phase regions surrounded by a binary Mo_{SS}–Mo_5SiB_2 eutectic.[17] Differences in the temperature gradient, degree of constitutional undercooling, and the growth velocity during the DS process have altered the established liquidus line,[12] leading to a fully eutectic growth. The liquidus-surface asymmetry of the Mo–Si–B system at the ternary eutectic point regarding the Mo_{SS}, Mo_3Si, and Mo_5SiB_2 phases also resulted in more-complex solidification behavior of eutectic Mo–Si–B alloys. The different slopes of the primary solidification surfaces of the phases will therefore have an influence on the coupled zone of the ternary eutectic growth.[12,30] The complex and dynamic phase transition during DS and growth of the ternary eutectic is the focus of the present in situ study using high-energy synchrotron radiation.
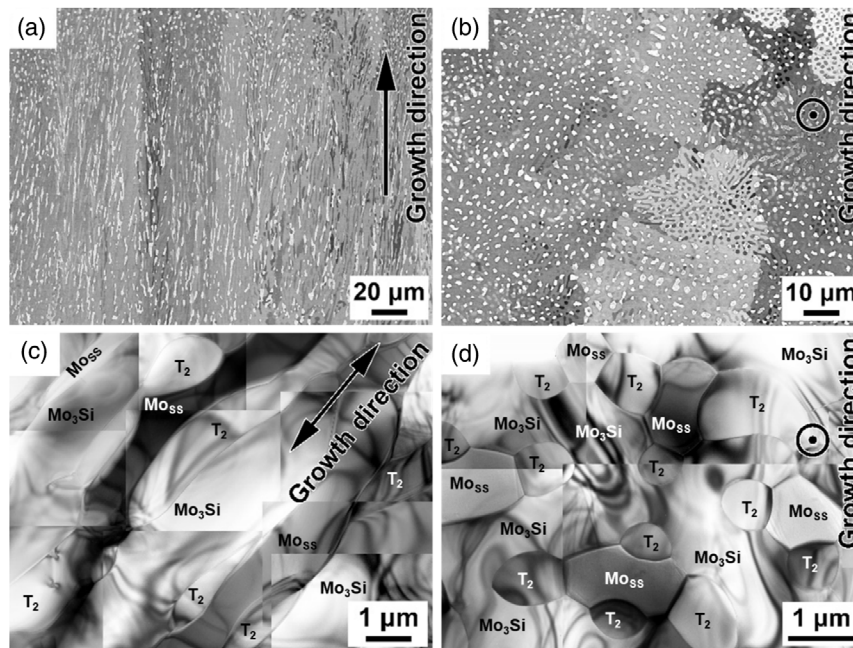
**ADVANCED
SCIENCE NEWS**

www.advancedsciencenews.com

**ADVANCED
ENGINEERING
MATERIALS**

www.aem-journal.com

Figure 2. Microstructures from longitudinal and transversal cross-sections of the directionally solidified ternary eutectic Mo–17.5Si–8B alloy; a) SEM b) BSE micrographs. c,d) bright-field TEM images. In the SEM–BSE micrographs, the light phase corresponds to Mo_{SS}, the gray phase corresponds to Mo_3Si, and the dark phase corresponds to Mo_5SiB_2 (T_2).

According to Kurz and Fisher,[19] a large temperature gradient and a slow growth velocity promotes a stable growth of eutectic compositions. Due to the asymmetry of the ternary eutectic reaction, resulting from different melting points of the Mo_{SS} (2623 °C[31]), Mo_3Si (2025 °C[32]), and Mo_5SiB_2 (2160–2200 °C[32]) phases and, thus, their different entropies of fusion, the temperature gradient during DS is the main factor and shifts the hypoeutectic alloy toward the coupled growth zone. A morphologically stable liquid–solid interface is formed in the coupled zone, which has slightly shifted toward the Mo_{SS} phase with the highest melting point.[19,30,33] Hence, the liquid–solid interface is kept at a low curvature of cellular growth and with a low perturbation of local undercooling, so that the eutectic phases grow in a stable manner parallel to the direction of the unidirectional temperature gradient.

3.2. In situ Observations during Liquid–Solid Transition

Figure 3 shows the raw data obtained during an in situ HEXRD measurement in the left column and the corresponding integrated diffractograms in the right column. The Debye–Scherrer diffraction rings are shadowed by parts of the DS machine in the lower part and on the left and right sides. For phase analysis, the upper right quarter was used. The reflections of the three different phases are marked in the integrated diffractograms. Figure 3a shows the HEXRD data directly before melting. The Debye–Scherrer diffraction patterns are continuous without any texture and the background of the integrated data shows a linear behavior. In contrast, Figure 3b shows data obtained directly in the melting zone without any defined reflex, which could be attributed to a crystal structure. The diffraction

pattern shows two diffuse rings. Correspondingly, the diffractogram appears with two diffuse peaks on the linear background, which were fitted with a Gaussian peak each. Furthermore, Figure 3c is obtained within the solidification front and shows the liquid–solid transition with about 80 vol% melt and 20 vol% crystalline phases. Accordingly, the diffractogram shows distinct peaks from the phases on top of the diffuse background peaks resulting from the melt. The crystallites appear with a texture indicated by nonhomogeneous-oriented intensity distribution on the Debye–Scherrer rings. Finally, the directional solidified condition with texture just below the melting temperature is shown in Figure 3d. Here, the diffractogram appears again with a linear background.

Figure 4 shows the determined phase fractions of the melt and of the three eutectic phases during the following states: during melting of the cast state (yellow region), in the liquid state (red region), during DS (orange region) and directly after entire (directed) solidification (blue region). With respect to experimental scatter, the volume fractions of the ternary eutectic are consistent with previous literature findings[17,34] and agree very well with the lever rule and volume fractions expected for the ternary eutectic point in the Mo-rich Mo–Si–B system located between 16–18 at% Si and 7–8 at% B.[12,17]

It has to be noted here, that the FlexiDS device uses two pyrometers for process control during directionally growth.[24] However, the positions are fixed within the induction coil (liquid zone) and at 10 mm above the coil and are, thus, not linked to the coordinate system of the positioning stage that moves the whole device up and down relative to the synchrotron X-ray beam. Hence, the increasing/decreasing volume fraction of the liquid phase was taken as a first indicator for the temperature in
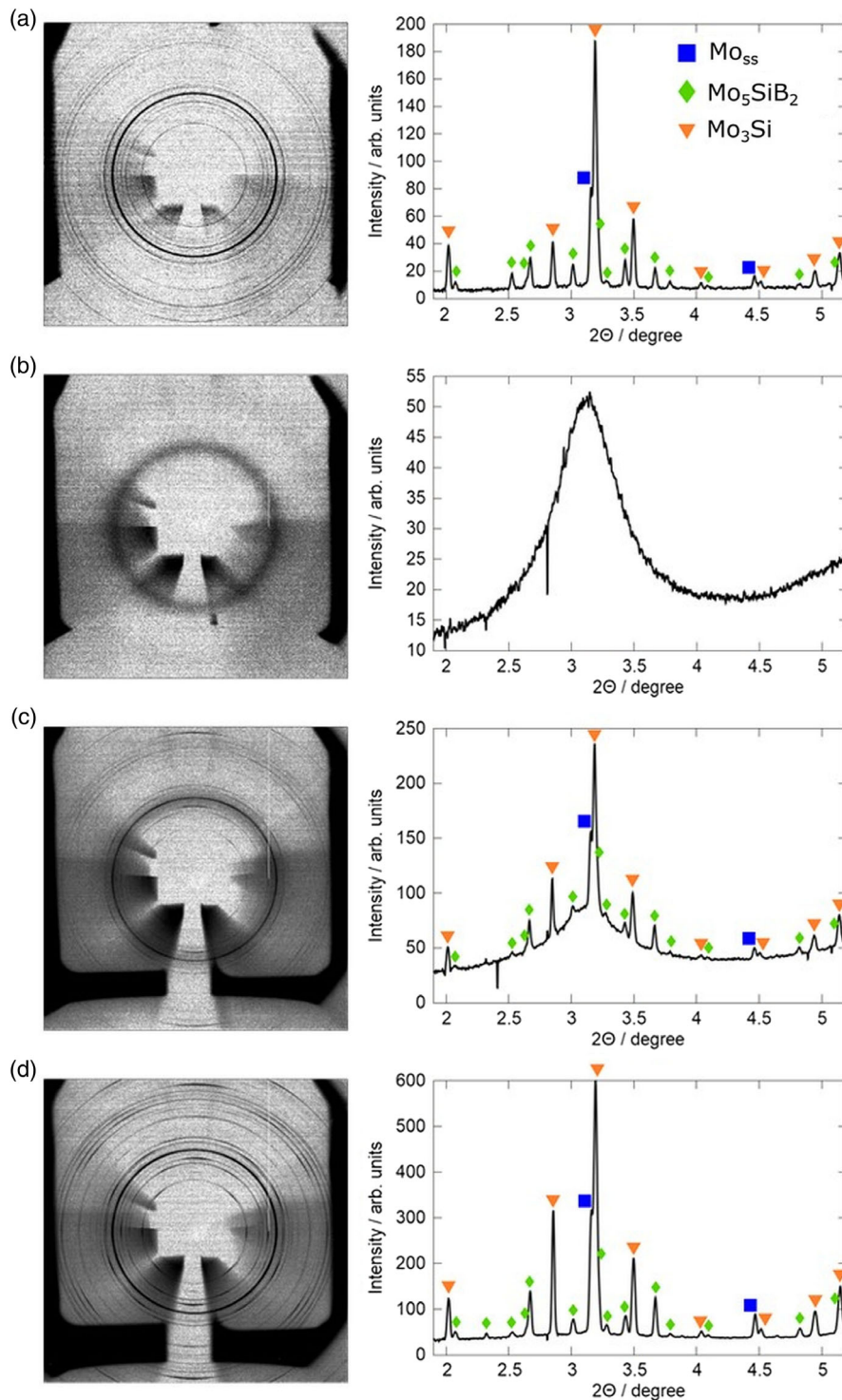
**ADVANCED
SCIENCE NEWS**

www.advancedsciencenews.com

*ADVANCED
ENGINEERING
MATERIALS*

www.aem-journal.com

Figure 3. In situ HEXRD data at different positions during DS processing. Left: Debye–Scherrer diffraction rings, right: the not normalized, integrated data of the upper right quarter of the diffraction rings, the three eutectic phases are marked, respectively. a) Solid state before melting without texture, b) liquid phase only, c) 80 vol% liquid and 20 vol% solid phases with texture, d) fully directional solidified microstructure just below the melting point with texture. In combination with Figure 3, it represents the benefit of the in situ synchrotron observations of the liquid–solid interface using the FlexiDS zone melting device at the P07 beam line.

Figure 4. After the sample was fully solidified, the decreasing lattice parameter "*a*" of the Mo_3Si phase was used as a second indicator for an indirect means of temperature determination. Mo_3Si was chosen since this phase represents the major phase
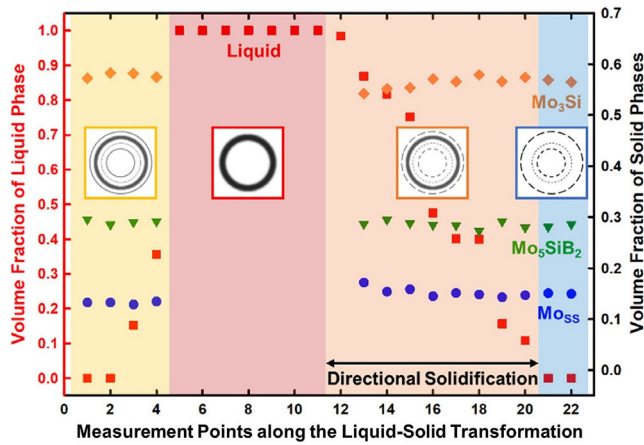
Figure 4. Fraction of the liquid and solid phases measured along the phase transformation and the eutectic solidification front during DS. Schematic Debye–Scherrer rings as detected during the in situ DS measurements are illustrated in addition.

Table 1. Lattice parameters of the in situ HEXRD experiments of DSed Mo–17.5Si–8B.

Phases	Symbols	This work [Å][a)]	DSed [Å][33]b)	As-cast [Å][33]b)
Mo$_{SS}$ (I m -3 m)	A	3.1784 ± 0.003	3.1380 ± 0.0001	3.1356 ± 0.0001
Mo$_3$Si (P m -3 n)	a	4.9708 ± 0.008	4.8971 ± 0.0002	4.8982 ± 0.0001
Mo$_5$SiB$_2$ (I 4/m c m)	a	6.1125 ± 0.01	6.0265 ± 0.0003	6.0267 ± 0.0000
	c	11.2287 ± 0.02	11.0684 ± 0.0007	11.0607 ± 0.0002

a)At temperatures just below the melting point; b)XRD data obtained at room temperature.

within the ternary Mo$_{SS}$–Mo$_3$Si–Mo$_5$SiB$_2$ eutectic and it is cubic, thus only one lattice parameter "*a*" has to be tracked. The average lattice parameters obtained from the in situ HEXRD measurements in Figure 4 are shown in **Table 1** and compared with recent experiments on DSed and as-cast Mo–17.5Si–8B.[33] The lattice parameter obtained recently at room temperature correlate quite well, whereas the slight differences may origin from different solidification velocities during solidification caused by the two different processing techniques. The higher lattice parameters obtained during the present in situ experiments are higher since they were taken from sample areas within the liquid–solid interface or from the already solidified crystals just below the melting point. During the liquid–solid transition via DS, all three solid phases simultaneously form out of the liquid phase. The fraction of the liquid phase is decreasing afterward. Independently from the fraction of the liquid phase that is present in the actually observed sample volume, the Mo$_{SS}$, Mo$_3$Si, and Mo$_5$SiB$_2$ phases grow with an almost constant ratio of their volume fractions relative to each other. This in situ observation is a strong experimental evidence for a coupled ternary eutectic growth in the Mo-rich Mo–Si–B system.

3.3. Crystallography and Texture of Constituent Phases after DS

The phase identification was obtained via EBSD mapping. **Figure 5** shows the phase map and IPF map of the DSed eutectic alloy Mo–17.5Si–8B in a longitudinal cut along the solidification direction. The IPF maps represent the orientation distribution relative to the normal direction (ND) of the observed sample's surface. In agreement with previous observations,[33] the Mo$_{SS}$ and Mo$_5$SiB$_2$ phases are elongated along the solidification direction with a slightly higher volume fraction of the Mo$_5$SiB$_2$ phase relative to the Mo$_{SS}$, Figure 5a. The eutectic cell boundaries can
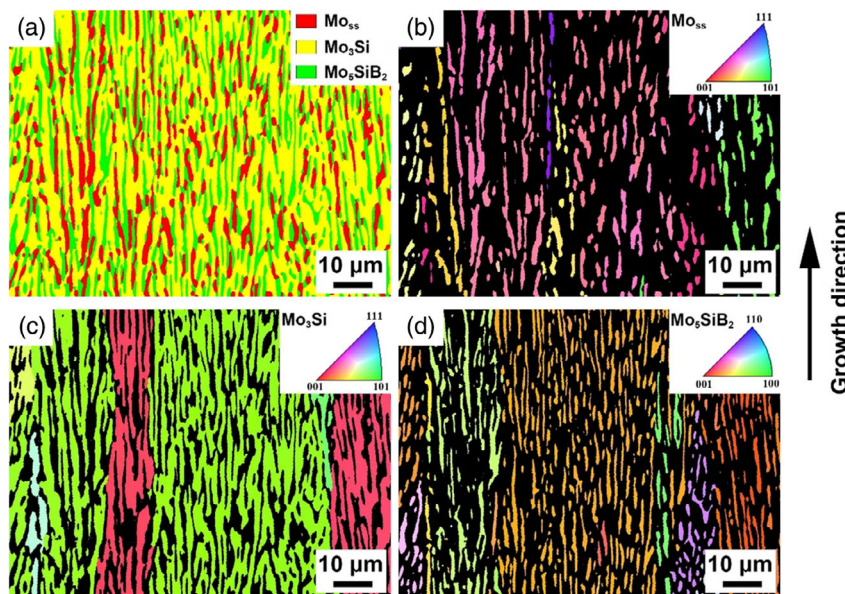

Figure 5. Typical phase map and corresponding ND a) IPF maps of the longitudinal section of the DSed alloy Mo–17.5Si–8B: phase map, IPF maps of b) Mo$_{SS}$, c) Mo$_3$Si, and d) Mo$_5$SiB$_2$. The ND is perpendicular to the observation surface.
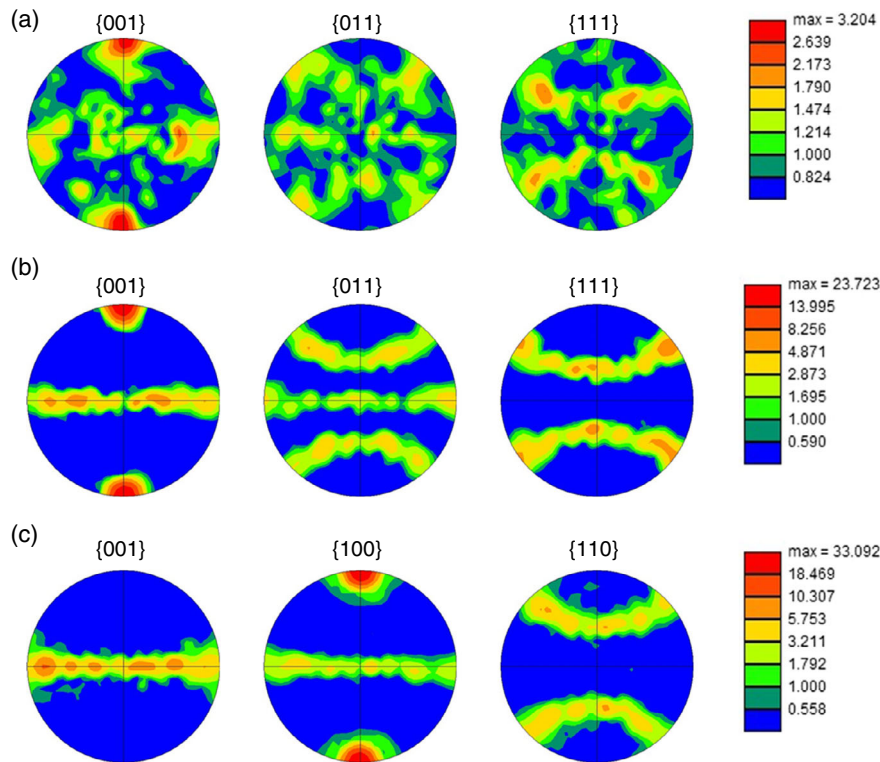
Figure 6. Pole figures of a) Mo_{SS}, b) Mo_3Si, and c) Mo_5SiB_2 in the longitudinal section of the directionally solidified Mo–Si–B alloy. The growth direction is the direction from bottom to top of the pole figures.

be identified from the phase orientations given in the IPF maps in Figure 5b–d. While the Mo_3Si and Mo_5SiB_2 phases possess a uniform orientation within the ternary eutectic cells, the orientation of the Mo_{SS} phase differs strongly. Thus, the eutectic cells can be identified by the common crystallographic orientation of Mo_3Si and Mo_5SiB_2 phases. In combination with the SEM–BSE images (Figure 2), the eutectic cells have typical diameters between 10 and 50 µm and are elongated well over 100–150 µm which is in absolute agreement with our recent investigations.[33]

Figure 6 shows the pole figures of the longitudinal section of the DSed alloy Mo–17.5Si–8B. Please note that the color scaling is different for the three sets of pole figures. The Mo_{SS} phase shows a weak <001> texture along the growth direction with low intensity, as shown in Figure 6a. Whereas the texture intensities of Mo_3Si and Mo_5SiB_2 were relatively high. The pole figure Figure 6b of the Mo_3Si phase demonstrated a strong preferred orientation of the <001> direction along the growth direction. Figure 6c shows the strong texture formation of the Mo_5SiB_2 phase. The Mo_5SiB_2 phase grew preferentially in the <100] direction with the {001} planes parallel to the growth direction, which is consistent with the microstructure reported by Uemura et al.[35,36] The eutectic phases had the preferential growth of <001>Mo_{SS}//<001>Mo_3Si//<100]Mo_5SiB_2 along the temperature gradient and the result agrees with texture recently evaluated.[33]

In addition, the pole figures calculated from the texture analysis of the HEXRD data are shown in **Figure 7**. For better comparability, the same orientations were chosen as for the pole figures obtained by EBSD. By matching the two methods, it is

clear that the observed texture is found throughout the sample and the EBSD measurements show a representative section. However, in comparison with the usual methods used to determine texture by HEXRD, it must be noted in this case that only a single image acquired during a 180° sample rotation was analyzed. In addition, only a 1 mm-wide sample volume in the center of the rotating bar was analyzed, resulting in a much sharper preferred orientation compared with a "normal" texture measurement.

4. Conclusion

A DS process was observed in situ with high-energy X-ray synchrotron measurements to study the growth behavior at the liquid–solid transition of a multicomponent alloy. To carry out these experiments, a new and unique sample environment "FlexiDS"[24] had been used to directly investigate crystal growth of the ternary eutectic Mo–Si–B alloys. Prior to DS, the eutectic alloy Mo–17.5Si–8B was prepared via arc-melting and cold crucible casting. During the DS process, high-energetic X-rays with a photon energy of 100 keV ($\lambda = 0.124$ Å) were used in transmission to obtain Debye–Scherrer diffraction rings. The diffraction rings were obtained within the liquid phase, the liquid–solid interphase and the solidified eutectic crystals by scanning multiple times through the observation volume of interest. It was found that: 1) During the liquid–solid transition, all three eutectic phases simultaneously form out of the solidifying liquid phase; 2) Independently from the fraction of the liquid phase that is present in the actually observed sample volume, the Mo_{SS},
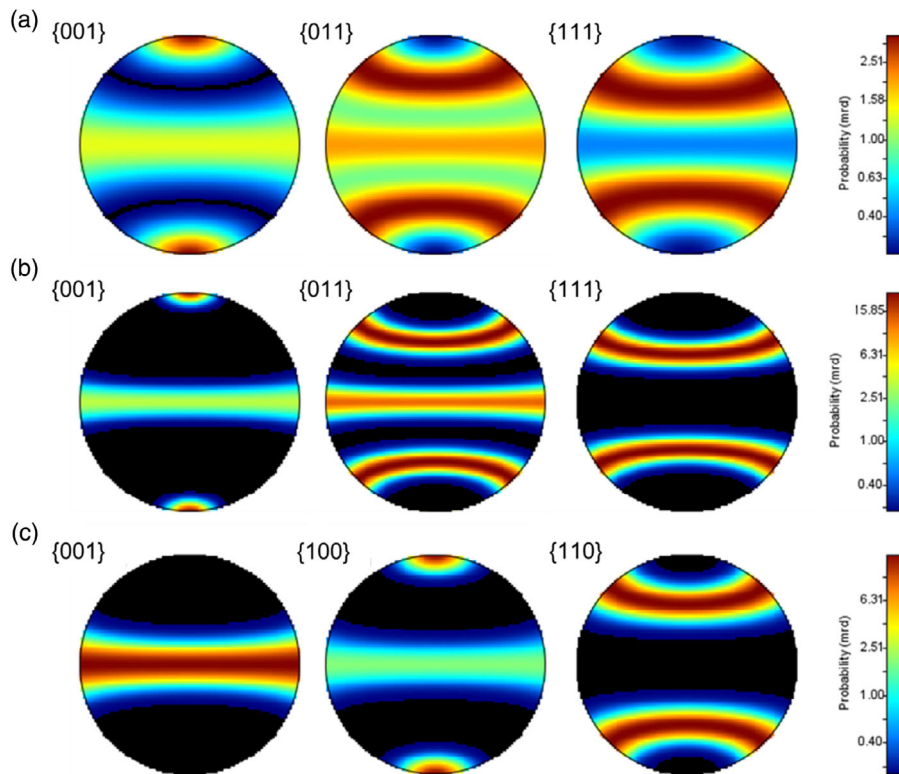
Figure 7. Pole figures of a) Mo_{SS}, b) Mo_3Si, and c) Mo_5SiB_2 in a 1 mm sample volume obtained during the in situ HEXRD measurements of the directionally solidified Mo–Si–B alloy.

Mo_3Si, and Mo_5SiB_2 phases grow with an almost constant ratio of their volume fractions relative to each other; 3) The in situ observation during DS provides an experimental evidence for a coupled ternary Mo_{SS}–Mo_3Si–Mo_5SiB_2 eutectic growth in the Mo–Si–B system; 4) Analyzing the DS texture formation by in situ HEXRD diffraction experiments could confirm EBSD texture analysis of the present experiments and recent work[33] showing preferential growth of the ternary eutectic of <001>Mo_{ss}// <001>Mo_3Si//<100]Mo_5SiB_2 along the solidification direction.

Conflict of Interest

The authors declare no conflict of interest.

Data Availability Statement

Research data are not shared.

[1] P. Jéhanno, M. Heilmaier, H. Saage, M. Böning, H. Kestler, J. Freudenberger, S. Drawin, *Mater. Sci. Eng.: A* **2007**, *463*, 216.

[2] T. A. Parthasarathy, M. G. Mendiratta, D. M. Dimiduk, *Acta Mater.* **2002**, *50*, 1857.

[3] M. G. Mendiratta, T. A. Parthasarathy, D. M. Dimiduk, *Intermetallics* **2002**, *10*, 225.

[4] J. H. Schneibel, J. J. Kruzic, R. O. Ritchie, in *Proc. 17th Annu. Conf. Foss. Energy Mater.* **2003**, Baltimore, MD **2003**.

[5] D. M. Berczik, *US Pat. 5,595,616; 5,693,156*, East Hartford, United Technol. Corp. **1997**.

[6] P. Jéhanno, M. Heilmaier, H. Kestler, *Intermetallics* **2004**, *12*, 1005.

[7] P. Jéhanno, M. Heilmaier, H. Kestler, M. Böning, A. Venskutonis, B. Bewlay, M. Jackson, *Metall. Mater. Trans. A* **2005**, *36A*, 515.

[8] M. Krüger, S. Franz, H. Saage, M. Heilmaier, J. H. Schneibel, P. Jéhanno, M. Böning, H. Kestler, *Intermetallics* **2008**, *16*, 933.

[9] D. Sturm, M. Heilmaier, J. H. Schneibel, P. Jéhanno, B. Skrotzki, H. Saage, *Mater. Sci. Eng.: A* **2007**, *463*, 107.

[10] M. Heilmaier, H. Saage, M. Krüger, P. Jéhanno, M. Böning, H. Kestler, *Mater. Res. Soc. Symp. Proc.* **2009**, *1128*, 4.

[11] K. Yoshimi, S. H. Ha, K. Maruyama, R. Tu, T. Goto, *Adv. Mater. Res.* **2011**, *278*, 527.

[12] G. Hasemann, S. Ida, L. Zhu, T. Iizawa, K. Yoshimi, M. Krüger, *Mater. Des.* **2020**, *185*, 108233.

[13] D. P. Mason, D. C. Van Aken, J. F. Mansfield, *Acta Metall. Mater.* **1995**, *43*, 1189.

[14] K. Ito, M. Kumagai, T. Hayashi, M. Yamaguchi, *Scr. Mater.* **2003**, *49*, 285.

[15] K. Fujiwara, H. Matsunoshita, Y. Sasai, K. Kishida, H. Inui, *Intermetallics* **2014**, *52*, 72.

[16] G. Hasemann, I. Bogomol, D. Schliephake, P. I. Loboda, M. Krüger, *Intermetallics* **2014**, *48*, 28.

[17] G. Hasemann, D. Kaplunenko, I. Bogomol, M. Krüger, *JOM* **2016**, *68*, 2847.

[18] J. Schmelzer, S.-K. Rittinghaus, A. Weisheit, M. Stobik, J. Paulus, K. Gruber, E. Wessel, C. Heinze, M. Krüger, *Int. J. Refract. Met. Hard Mater.* **2019**, *78*, 123.

[19] W. Kurz, D. J. Fisher, in *Fundamentals of Solidification*, Trans. Tech. Publ. **1992**, p. 88.

[20] D. P. Mason, D. C. Van Aken, *Acta Metall. Mater.* **1995**, *43*, 1201.

[21] F. Wang, A. Shan, X. Dong, J. Wu, *J. Alloys Compd.* **2008**, *462*, 436.

[22] H. Bei, G. M. Pharr, E. P. George, *J. Mater. Sci.* **2004**, *39*, 3975.

[23] H. Gier, M. Beyss, *Eurpean Patent EP0345542B1*, **1989**.

[24] C. Gombola, G. Hasemann, A. Kauffmann, I. Sprenger, S. Laube, A. Schmitt, F. Gang, V. Bolbut, M. Oehring, M. Blankenburg, N. Schell, P. Staron, F. Pyczak, M. Krüger, M. Heilmaier, *Rev. Sci. Instrum.* **2020**, *91*, 093901.

[25] A. P. Hammersley, S. O. Svensson, M. Hanfland, A. N. Fitch, D. Hausermann, *High Press. Res.* **1996**, *14*, 235.

[26] S. Merkel, http://merkel.zoneo.net/RDX/index.php (accessed: December 2013).

[27] L. Lutterotti, M. Bortolotti, G. Ischia, I. Lonardelli, H.-R. Wenk, De Gruyter, Berlin, Boston **2007**, 125.

[28] K. Hauschildt, A. Stark, H. Burmester, U. Tietze, N. Schell, M. Müller, F. Pyczak, *Mater. Sci. Forum* **2018**, *941*, 943.

[29] P. H. Hermans, A. Weidinger, *Die Makromol. Chem.* **1961**, *44*, 24.

[30] W. Kurz, P. R. Sahm, in *Gerichtete Erstarrung Eutektischer Werkstoffe*, Springer-Verlag, Berlin, Heidelberg, NY **1975**, p. 106.

[31] A. B. Gokhale, G. J. Abbaschian, *J. Phase Equilibria* **1991**, *12*, 493.

[32] R. Mitra, *Int. Mater. Rev.* **2006**, *51*, 13.

[33] L. Zhu, S. Ida, G. Hasemann, M. Krüger, K. Yoshimi, *Intermetallics* **2021**, *132*.

[34] G. Hasemann, M. Krüger, M. Palm, F. Stein, *Mater. Sci. Forum* **2018**, *941*, 827.

[35] S. Uemura, T. Yamamuro, J. W. Kim, Y. Morizono, S. Tsurekawa, K. Yoshimi, *J. Jpn. Inst. Met.* **2016**, *80*, 529.

[36] S. Uemura, S. Y. Kamata, K. Yoshimi, S. Tsurekawa, *High Temp. Mater. Process.* **2020**, *39*, 136.